International Micro Air Vehicle Conference and Flight Competition (IMAV2013)
17-20 September 2013, Toulouse, France

Vector thrust multi-rotor copter and its application for building inspection

C.-H. Kuo[1], C.-M. Kuo[1], A. Leber[1] and C. Boller[1,2]

[1] Saarland University, Mat. Sc. & Technol. Dept., Chair in NDT & QA, Saarbrucken, Germany
[2] Fraunhofer Inst. for NDT (IZFP), Saarbrucken, Germany

Abstract

Multi-rotor copters are becoming increasingly popular for research and experimen-tation of air vehicle control, aerial imaging (photo/video) and even the hobby market, due to its excellent performance and mechanical downscaling as well as cost when compared to its conventional full scaled and possibly even manned siblings. The re-search groups at both Fraunhofer IZFP and Saarland University have carried out ex-periments, using a multi-rotor copter with an off the shelf camera for building in-spection (aerial photo) for years [1]. With possibly all of the conventionally built ro-tary wing micro aerial vehicles (MAV) the translation of the vehicle in any direction will cause the vehicle to tilt its body, which leads to distortion of images/photos even with an integrated gimbal system as a tool for image stabilization. In order to keep the vehicle in a stable, horizontal position even during translation, a novel vector thrust system has been designed, analyzed through use of numerical simulations, and proven by means of hardware realization and experimental flights. The first part of this paper discusses the modeling of the vector thrust system using a plus- and x-configuration. The second half of the paper consists of the numerical simulation to prove the concept. The last part describes demonstration of the concept with real hardware and experimental flight results.

Glossary:
F_x, F_y, F_z**=Force in X,Y,Z direction (body axis)**
w_i**=rotational speed of motor i**
ϕ**,** θ**,** ψ**=Roll,Pitch and Yaw angle (attitude)**
cϕ**,** θ**,** ψ**.s**ϕ**,** θ**,** ψ**= cos**ϕ **or** θ **or** ψ**.sin**ϕ **or** θ **or** ψ
b=Lift constant
d=Drag constant

1 Introduction

An enhanced amount of civil infrastructure buildings (including roads and bridges) has become an issue with regard to the ageing process and hence a resulting life cycle management. According to the Federal Highway Administration (FHWA), nearly 70% of all bridges and roads need to be inspected regularly in the US [2, 3, 4, 5, 6]. This in-spection is based on purely visual methods and is completed by inspection personnel present on site [7, 8, 9]. However, apart from bridges, no institution is estimating the number of required inspections and methods with regard to infrastructures such as government buildings or factories. However, the inspection of certain structures can be dangerous for inspectors to be on site, as some locations on the structure may only be accessed under extreme circumstances, such as very slender, high towers [10, 11, 12, 13]. Since most inspections refer to visual inspection (95%) a robot, equipped with a digital camera, instead of a human inspector is proposed

to be used. An octocopter is a fairly popular solution and was hence used throughout this project, as it offers sufficient payload capacity, is small in size, and most importantly, is comparatively simple with regard to the mechanical structure. (Fig. 1)

Diameter	1.02 m
Take-Off Weight	2.5 kg
Endurance	< 20 min
Max. Payload	2 kg

Figure 1: Octocopter used and technical data

The first inspection task took place at the Fraunhofer IZFP building in Saarbrucken/Germany (Fig. 2). The total inspection took less than 8hr (which con-sisted of time for the actual flight and photo checking). The results of the inspection, in form of images of each facade combined in a 3D model, can be seen in Fig. 3

Figure 2: **Left**: Aerial view of Fraunhofer IZFP with rendered line indicate inspection facade.
Right: Front view of the Fraunhofer IZFP.

The inspection mission was significantly faster than a conventional inspection would have been. There were around 4GB of photo material collected for each facade of the building. However, only around 10% of the photos were selected for the image processing in the end. The rest was considered as 'noise' since different of the imag-es showed the same however with a slight variation in attitude (Fig. 4).
Even though the octocopter was equipped with a gimbal system, attitude fluctua-tion still affects the image captureD, therefore reducing the 'noise' resulting from attitude variation becomes important to further enhance the imaging process.

2 Vector thrust propulsion for robot (reduction of attitude noise while in action)

Any translation in x, y and z direction of the MAV will require attitude change [14, 15, 16], due to the fact that the motions are all controlled by a difference in rotation speed of the motors (Fig. 5).

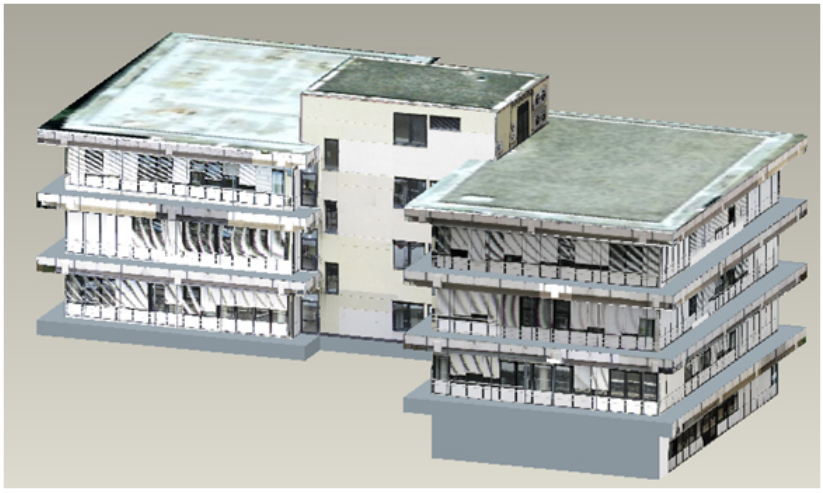

Figure 3: 3D CAD model of inspected building (Fraunhofer IZFP)

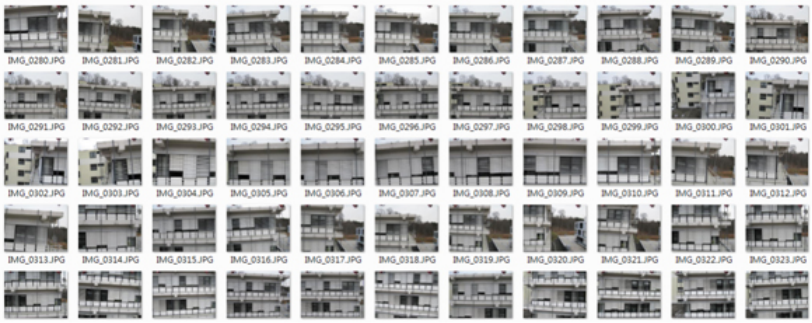

Figure 4: Few % of photos taken as an example to show variation in attitude

This attitude change is a source of noise during the image capturing process (even with a camera gimbal stabilization, attitude change still has a very large effect). However, translation in any x, y and z direction is required for the inspection. Therefore a vector thrust system is proposed in order to remove atti-tude changes when a motion is applied to the multi-rotor vehicle.

Vector thrust in the type of rotary wing vehicle shown above can be realized by twisting the rod along which the rotor is attached, hence around the x- and y-axis respectively when taking the definitions provided in Fig. 5(left). To describe the di-rection of motion of the aerial vehicle itself the position of rotors versus the direction of motion of the aerial vehicle itself becomes important. In the case of four rotors and when the aerial vehicle moves in the direction of either the x- or y-axis within the x-y-plane the configuration will be called a plus-configuration while when the aerial vehicle moves in a direction between the x- and y-axis it will be called an x-configuration. Comparing the two configurations it already becomes obvious that efficiency with respect to vehicle stabilization becomes less in the plus-configuration since two of the vector thrust rotors along the direction of motion basically do not show any effect. Within the following the analytical modeling of the two

configura-tions will be described before applying the models along simulations.

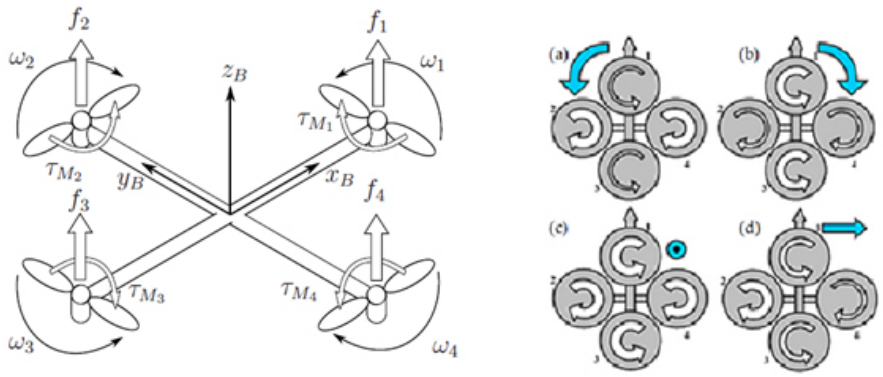

Figure 5: **Left**: Free force diagram of the multi-rotor robot (quad). **Right**: Motion diagram, a) yaw anti-clockwise, b) yaw clockwise,c) increase altitude (movement in Z direction only),d) roll positively to create motion in y direction (negatively).

3 Modeling of plus frame vector thrust

Lift force on each motor is

$$L_i = F_i b w_i \tag{1}$$

Torque of each motor is

$$\tau_i = d w_i \tag{2}$$

6 DOF generalized vector q

$$q = \begin{bmatrix} x & y & z & \phi & \theta & \psi \end{bmatrix}^T \tag{3}$$

The Lagrangian is obtained by modeling the energy of the system which is the differ-ence between kinetic and potential energy.

$$L = T - U \tag{4}$$

Where T is the kinetic energy and U is the potential energy. The final expression is:

$$L(q,q) = \frac{\dot{1}}{2} m(\dot{x} + \dot{y} + \dot{z}) + \frac{1}{2}(I_{xx}\dot{\phi}^2 + I_{yy}\dot{\theta}^2 + I_{zz}\dot{\psi}^2) - mgz \tag{5}$$

If an external generalized force is applied:

$$F = \frac{d}{dt}\frac{\partial L}{\partial \dot{q}} - \frac{\partial L}{\partial q} \tag{6}$$

$$F = [F_\xi \ \tau]^T \tag{7}$$

$$F_\xi = [F_x \ F_y \ F_z]^T \tag{8}$$

$$\tau = [\tau_\phi \ \tau_\theta \ \tau_\psi]^T \tag{9}$$

Where :

$$F_x = \sum F_{m2\&4} = -b(w_2^2 \ + \ w_4^2)sin\theta_s$$

$$F_y = \sum F_{m1\&3} = -b(w_1^2 \ + \ w_3^2)sin\phi_s$$

$$F_z = \sum F_{m2 \ to \ 4} = -b[(w_2^2 \ + \ w_4^2)cos\,|\theta_s| + (w_1^2 \ + \ w_3^2)cos\,|\phi_s|] \tag{10}$$

The PDE of $\frac{d}{dt}\frac{\partial L}{\partial \dot{q}}$ and $\frac{\partial L}{\partial q}$ can be expressed as follows:

$$\frac{d}{dt}\frac{\partial L}{\partial \dot{q}} = \begin{bmatrix} m\ddot{x} \\ m\ddot{y} \\ m\ddot{z} \\ I_{xx}\ddot{\phi} + \dot{I}_{xx}\dot{\phi} \\ I_{yy}\ddot{\theta} + \dot{I}_{yy}\dot{\theta} \\ I_{zz}\ddot{\psi} + \dot{I}_{zz}\dot{\psi} \end{bmatrix}$$

and

$$\frac{\partial L}{\partial q} = \begin{bmatrix} 0 & 0 & -mg & 0 & 0 & 0 \end{bmatrix}^T \tag{11}$$

Now, the force from the body frame must be translated to a global frame by using the rotational matrix R.

$$\frac{\partial L}{\partial q} = \begin{bmatrix} c\theta c\psi & c\theta s\psi & \text{-}s\theta \\ s\phi s\theta c\psi - c\phi s\psi & s\phi s\theta s\psi + c\phi c\psi & s\phi c\psi \\ c\phi s\theta c\psi + s\phi s\psi & c\phi s\theta s\psi + s\phi c\psi & c\phi c\psi \end{bmatrix} \tag{12}$$

Note:

$$F_\xi = R.F_{rotor} \tag{13}$$

$$\tau_\phi = (F_{2z} - F_{4z})l + (\tau_2 + \tau_4)sin\theta_s \tau_\theta = (F_{3Z} - F_{1Z})l + (\tau_1 + \tau_3)sin\theta_s$$

$$\tau_\psi = (\tau_1 + \tau_3)cos\,|\phi_s| + (\tau_2 + \tau_4)cos\,|\theta_s| \tag{14}$$

Where $(\tau_2 + \tau_4)sin\theta_s$ & $(\tau_1 + \tau_3)sin\phi_s$ are very small turns, which can be assumed to be zero. Thus, the Euler-Lagrange equation with (7, 8, 9, 10, 11, 13 and 14) together yield to:

$$\ddot{q} = \begin{pmatrix} \frac{F_x c\theta c\psi + F_y c\theta s\psi - F_z s\theta}{m} \\ \frac{F_x(s\phi s\theta c\psi - c\phi s\psi) + F_y(s\phi s\theta s\psi - c\phi c\psi) - F_z s\phi c\theta}{m} \\ \frac{F_x(c\phi s\theta c\psi - s\phi s\psi) + F_y(c\phi s\theta s\psi - s\phi c\psi) - F_z c\phi c\theta}{m} - g \\ \frac{(b(w_2^2 - w_4^2)cos|\theta_s|)l - \dot{I}_{xx}\dot{\phi}}{I_{xx}} \\ \frac{(b(w_3^2 - w_1^2)cos|\phi_s|)l - \dot{I}_{yy}\dot{\theta}}{I_{yy}} \\ \frac{d[(w_3^2 + w_1^2)cos|\phi_s| - (w_3^2 + w_1^2)cos|\theta_s|] - \dot{I}_{zz}\dot{\psi}}{I_{zz}} \end{pmatrix} = \begin{pmatrix} \ddot{x} \\ \ddot{y} \\ \ddot{z} \\ \ddot{\phi} \\ \ddot{\theta} \\ \ddot{\psi} \end{pmatrix} \tag{15}$$

Since the robot is at near hover condition, $\dot{I}_{xx}\phi$, $\dot{I}_{yy}\theta$ and $\dot{I}_{zz}\psi$ are equal to zero.

Clearly Eq.s (10 & 15) show that the generation of a yaw moment is unavoidable if the vector thrust is active. However, these equations of motion do not consider any input from the autopilot (ie assuming autopilot is inactive).

3.1 Plus-configuration vector thrust numerical simulations

Fig. 5 shows the MAV with the respective coordinate system. It is assumed that one desires a translation in y-direction. In order to carry out this motion without a change in roll angle, two servos attached to the motors 1&3 (Fig. 5 Right) must be active (in this case servos are set to be 5 degrees at the beginning). All motors rotate at a constant speed.

The simulation results displayed in Fig. 6 show that creation of a yaw moment is pos-sible while the vector thrust is active. No autopilot is involved. The flight control sys-tem does have heading (yaw) angle lock capabilities in this case. Fig. 7 shows the simulation results when both autopilot and vector thrust are active. The global translation is now limited to y and z (z is altitude), and x has been completely re-moved by locking the heading angle.

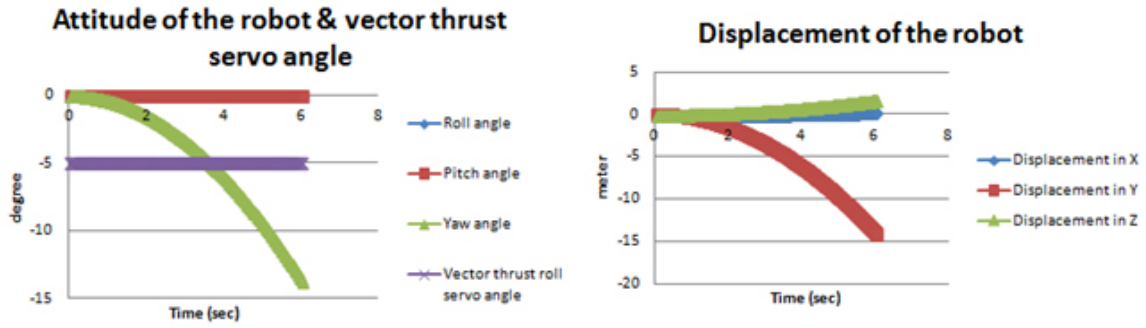

Figure 6: **Left**: Attitude change of robot when vector thrust is applied. **Note**: no change in roll and pitch, but yaw change is undesirable (cause of symmetric rotation of motor2&4 (Fig. 3.Right) **Right**: Global translation of robot. Note: y-direction is desirable, and x-direction is causing by unde-sired yaw.

4 X-configuration for vector thrust modeling

The main reason for the plus-configuration frame robot to shift its heading every time vector thrust becomes active is because asymmetry of the vector thrust servo and rotor rotation direction. However, this problem will not occur when using an x- configuration robot. For application of vector thrust, all motors rotate partially also around the x-axis to allow a momentum around the y-axis and rotate around y-axis to allow a momentum around the x-axis. All equations except for Eq.s (10), (14) and

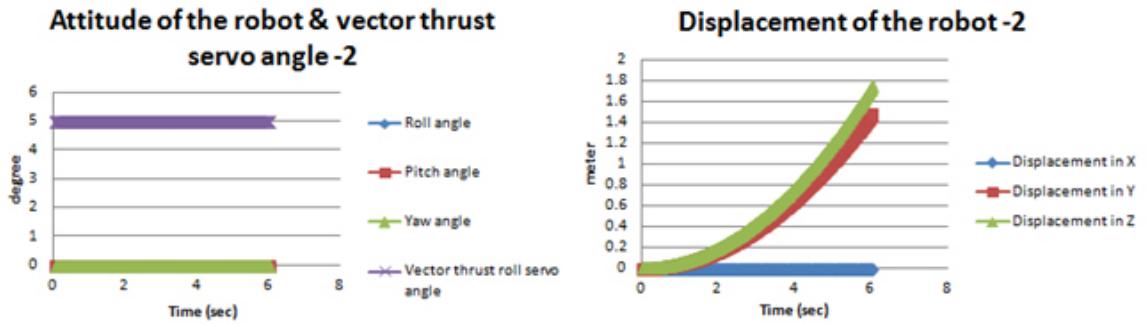

Figure 7: **Left**: Attitude change of robot when vector thrust is applied. **Right**: Global translation of robot. Note: no any undesirable translation in x-direction.

(15) are valid (since the motor numbering and orientation change; see Fig. 8). The modified equations are Eq.s (16), (17) and (18) respectively.

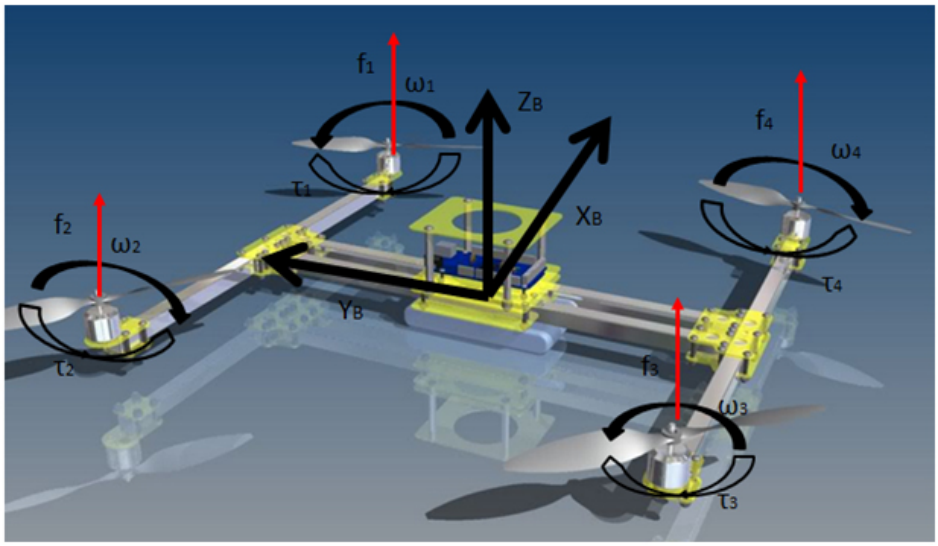

Figure 8: Shows force diagram of X-frame setup Quad-copter. Note: here we use H-frame because of simplicity for installation of vector thrust servo.[17].

$$F_x = -b(w_1^2 + w_2^2 + w_3^2 + w_4^2)sin\theta_s$$

$$F_x = b(w_1^2 + w_2^2 + w_3^2 + w_4^2)sin\phi_s$$

$$F_z = b(w_1^2 + w_2^2 + w_3^2 + w_4^2)\ cos|\theta_s|\ cos|\phi_s| \tag{16}$$

$$\tau_\phi = (F_{1Z} + F_{2Z} - F_{3Z} - F_{4Z})lcos45 + (\tau_1 + \tau_2 + \tau_3 + \tau_4)sin\theta_s$$

$$\tau_\theta = (F_{1Z} + F_{2Z} - F_{3Z} - F_{4Z})lcos45 + (\tau_1 + \tau_2 + \tau_3 + \tau_4)sin\phi_s$$

$$\tau_\psi = (\tau_1 + \tau_2 + \tau_3 + \tau_4)\ cos|\phi_s|\ cos|\theta_s| \tag{17}$$

$$\ddot{q} = \begin{pmatrix} \frac{F_x c\theta c\psi + F_y c\theta s\psi - F_z s\theta}{m} \\ \frac{F_x(s\phi s\theta c\psi - c\phi s\psi) + F_y(s\phi s\theta s\psi - c\phi c\psi) - F_z s\phi c\theta}{m} \\ \frac{F_x(c\phi s\theta c\psi - s\phi s\psi) + F_y(c\phi s\theta s\psi - s\phi c\psi) - F_z c\phi c\theta}{m} - g \\ \frac{(b(w_1^2+w_2^2-w_3^2-w_4^2)cos\theta_s cos\phi_s)lcos45 - d(w_2^2+w_4^2-w_1^2-w_3^2)sin\theta_s - \dot{I}_{xx}\dot{\phi}}{I_{xx}} \\ \frac{(b(w_3^2+w_2^2-w_1^2-w_4^2)cos\theta_s cos\phi_s|)lcos45 - d(w_2^2+w_4^2-w_1^2-w_3^2)sin\phi_s - \dot{I}_{yy}\dot{\theta}}{I_{yy}} \\ \frac{d(w_1^2+w_2^2+w_3^2+w_4^2)cos\theta_s cos\phi_s - \dot{I}_{zz}\dot{\psi}}{I_{zz}} \end{pmatrix} = \begin{pmatrix} \ddot{x} \\ \ddot{y} \\ \ddot{z} \\ \ddot{\phi} \\ \ddot{\theta} \\ \ddot{\psi} \end{pmatrix} \tag{18}$$

where again, near hover condition, therefore $\dot{I}_{xx}\dot{\phi}$, $\dot{I}_{yy}\dot{\theta}$ and $\dot{I}_{zz}\dot{\psi}$ are equal to zero.

4.1 X-configuration vector thrust numerical simulation

Using Eq. (18) and assuming all 4 motors to rotate at the same speed the vector thrust roll servo angle is set to 5X and the vector thrust pitch servo angle to 0X. In this case the autopilot is inactive, thus no control for heading lock is used.

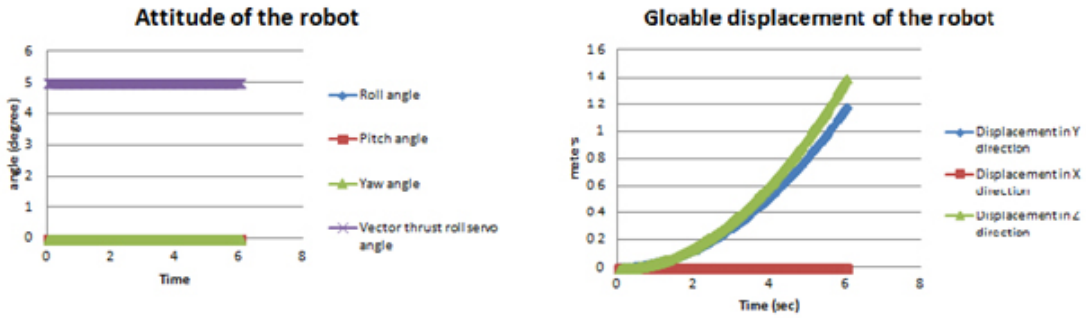

Figure 9: **Left**: Numerical simulation results of robot attitude when vector thrust roll servo is active at 5 degree. (**Note**: no autopilot control). **Right**: global displacement of the robot. **Note**: no undesired x displacement due to no yaw angle created.

Numerical simulation results displayed in Fig. 9 show that the performance of vector thrust using the x-configuration is much better (stable, without any input of autopilot) than the plus-configuration. However, the only problem is the actual design of an x-configuration vector thrust quadcopter as it may require 6 servos instead of 4 when the specific H-frame will be used as shown in Fig. 8.

5 Hardware realization and test flight

In order to confirm the numerical simulation, a simple cross-framed quadcopter was built as shown in Fig. 10 which could be flown in the plus- as well as the x-configuration. Flight tests were performed with the different configurations where videos have been taken from which at least two frames have been selected from the x-configuration flight and are shown in Fig. 11. When comparing the two pictures it can be seen that the vehicle stays continuously horizontal with no significant yaw being observed irrespective of the vehicle hovering or moving. This enhancement in attenuation therefore significantly helps to reduce the 'noise' with respect to the series of images taken.

Figure 10: **Left**: overview of the vector thrust Quad-copter. **Right**: note how the motor 1 and 3 tilt.

Figure 11: **Left**: hovering and vector thrust is activated. **Right**: 2 seconds after activation. Note: the quad moved in Y-axis without any attitude change.

6 Conclusion and future work

It has been shown that vector thrust propulsion of a multi-copter aerial vehicle does have a significant advantage on enhancing the attitude of the vehicle and hence the quality of any images taken from that vehicle with any type of sensing system. The analytical approach proposed can be programmed and implemented into the flight control of the aerial vehicle and first experiments performed indeed demonstrate the enhancement of the vehicle's attitude performance. As to the possible control approaches the x-configuration is definitely superior when compared to the plus-configuration. With the enhancement in attitude achieved it will now be the next steps to equip the aerial vehicle with the sensing system (i.e. a camera) and to observe up to which extent the gains are in terms of 'noise' obtained from the redundant images taken. There is also a drawback from the vector thrust application which can be seen from Fig. 7. With increasing time there is an increase in speed which results

in acceleration and which will theoretically lead to a gradual reduction of image quality. However how serious this effect is in reality needs to be proven by experiment and in the worst case this could be compensated through an additional velocity control. This concept has applied to the European Patent Office[18].

References

[1] C.-H. Kuo, A. Leber, C.-M. Kuo, C. Boller, C. Eschmann and J. Kurz. Unmanned robot system for Structure health monitoring and Non-Destructive Building Inspection, current technologies overview and future improvements; Proc. of the Internat. Workshop on SHM, Stanford Univ., Stanford/CA, USA, September 2013

[2] Golabi K, Thompson P, Hyman W. Pontis. A network optimization system for bridge improvements and maintenance Technical manual. Publication number FHWA-SA-94-031: US Department of Transportation, Federal Highway Administration; 1993.

[3] Brecher A.. Infrastructure: a national priority. Soc Women Eng 1995; 4(16):14-16.

[4] Roberts E, Shepard R.. Bridge management for the 21st century. Transport Res Rec 2000;1696:197-203.

[5] Bridge Inspection Robot Development Interface (BIRDI). Development of high-tech automatic robot system for bridge inspection and monitoring, Technical report for Ministry of Construction and Transportation (in Korean), 2007.

[6] Federal Emergency Management Agency (FEMA). Module 1C structural engineering, structural collapse technician course - student manual 8 `http://www.fema.gov/emergency/usr/sctc.shtm20098`(last visit Dec, 2009)

[7] Aldunate R., S.F. Ochoa, F. Pena-Mora, M. Nussbaum. Robust mobile ad hoc space for collaboration to support disaster relief efforts involving critical physical infrastructure, Journal of Computing in Civil Engineering 20 (1) (2006) 13-27.

[8] Federal Highway Administration (FHWA). Bridge Inspections Training Manual, July 1991.

[9] Bridge Maintenance Training Manual. US Federal Highway Administration, FHWAHI-94-034, Prepared by Wilbur Smith Associates, 1992.

[10] NJDOT, Bridge Inspection Work Zone. Setup Guide, 2009. `http://www.state.nj.us/`

[11] Shibata T. and A. Shibata. Summary report of research and study on robot systems for maintenance of highways and bridges, Robot, vol. 118, JARA, Tokyo, Japan, Sep. 1997, pp. 41-51.

[12] Product Catalog. Paxton-Mitchell Snooper? Series 140 `http://www.paxtonmitchell.com`

[13] Oh J.-K., A.-Y. Lee, S.M. Oh, Y. Choi, B.-J. Yi, H.W. Yang. Design and control of bridge inspection robot system, IEEE Int. Conf. on Mechatronics and Automation, Aug. 2007, pp. 3634-3639.

[14] Luukkonen T. Modelling and control of quadcopter; School of Science. Independent research project in applied mathematics Espoo, August 22, 2011. Aalto University.

[15] Group 10833. "Modelling and Control of Autonomous Quad-Rotor". 2nd Semester Project of the Intelligent Autonomous Systems Master Programme Faculty of Engineering, Science and Medicine. University of Aalborg, Denmark June 2010.

[16] Naidoo Y., R. Stopforth and G. Bright. Quad-Rotor Unmanned Aerial Vehicle Helicopter Modelling & Control; Intech open access publisher. Aug 2011

[17] X-configuration in H-Frame `http://aeroquad.com/showthread.php?4560-My-new-H-frame-design/page2`(last visit Nov, 2012)

[18] European Patent Office, Submission number: 2288267, Application: EP13183347.7, Reference Code: F54634-EP